Thin-Walled Structures 118 (2017) 37–45

Contents lists available at ScienceDirect

Thin-Walled Structures

journal homepage: www.elsevier.com/locate/tws

Full length article

Optimum design of aircraft panels based on adaptive dynamic harmony search

Behrooz Keshtegar[a], Peng Hao[b,*], Yutian Wang[b], Yangfan Li[b]

[a] Department of Civil Engineering, University of Zabol, P.B. 9861335-856 Zabol, Iran
[b] State Key Laboratory of Structural Analysis for Industrial Equipment, Department of Engineering Mechanics, Dalian University of Technology, 116023 Dalian, China

ARTICLE INFO

Keywords:
Adaptive dynamic harmony search
Aircraft panels
Buckling
Optimization
Weight

ABSTRACT

Aiming at the optimization of aircraft panels, a modified version of harmony search (HS) algorithm is proposed based on the information of the harmony memory (a memory location where all the solution vectors are stored) for improvisation procedure, named as adaptive dynamic harmony search (ADHS) algorithm. In order to reduce the amount of calculation, response surface method is employed, and second-order polynomial with cross terms is used to construct the model. To demonstrate the advantage of the proposed algorithm, typical aircraft panels under buckling constraint are established, and several existing HS algorithms are compared. The effects of the number of improvisation (*NI*) and harmony memory size (*HMS*) are investigated and discussed in detail. Results indicate that the proposed ADHS can provide an optimum design in a robust manner, and local optimum solutions may be reduced based on the ADHS for optimization problems with multiple local minima. Finally, several useful information is obtained for the design of stiffened panels with cutouts.

1. Introduction

Due to high specific strength and stiffness, stiffened panels are widely used in various types of weight-critical applications to resist buckling and collapse, such as aircrafts and launch vehicles, etc. For a variety of reasons, e.g. easy access, inspection, etc, cutouts are usually inevitable for aircraft structures [1–7], which may cause remarkable reductions on both load-carrying capacity and structural efficiency. To compensate the performance loss caused by cutout, the topic on the design of stiffened shells with cutouts becomes ever more significant and urgent.

In the past, many researchers have undertaken the research on the buckling behavior of thin-walled panels with cutouts. Mahmoud et al. [8] studied the steel cylindrical shells with various sizes of elliptical cutouts under axial compression. Schlack et al. [9] determined the buckling load of square plates with a circular central hole by experiment, and the results agree well with the predictions by the Ritz energy method. Later, Tennyson [10] found that the membrane stress concentration factors of circular cylindrical shells under axial compression increase rapidly with the growth of curvature parameter. Until now, many investigators have investigated the effects of cutouts on the metal shells or composite shells [11–13]. To mitigate the decline of load capacity and stability caused by cutouts, much attention was paid to the thin-wall structures reinforced by stiffeners [14–16]. It is worth noting that those works mentioned above are mainly focused on straight stiffeners, and their enhancement approach is relatively fixed. The primary reasons that cause this situation mainly include the limitation of current manufacturing technology and design method. As for this, for certain types of aircrafts, the cutout are still reinforced by straight stiffeners [17,18], which are easy for manufacturing, assembly, inspect and design optimization. Fortunately, as manufacturing technologies are developed rapidly, new manufacturing processes (e.g. additive manufacturing) make it more convenient to reinforce thin-wall structures by curvilinear stiffeners, which can greatly enhance the load-carrying capacity. However, for the design optimization of curvilinear stiffeners, it is still a very challenging problem due to the high-dimensional inherence. Kapania et al. [19] summarized the previous research works of curvilinear stiffened panels, and found that curvilinearly stiffened panels have larger design space as well as lightweight potential in comparison with straight stiffeners. As for recent works, more and more researches are focused on the mechanical behavior of curvilinearly stiffened panels under shear load or combined compression-shear load. For instance, the mesh-free method is used to study the buckling and static behavior of curvilinearly stiffened panels [20,21]. Wang et al. [22] performed the buckling optimization of curved stiffeners based on a global/local coupled strategy, and a significant improvement of post-buckling performance was observed. In addition, a new shear deformation theory was developed for functionally graded

* Corresponding author.
E-mail address: haopeng@dlut.edu.cn (P. Hao).

http://dx.doi.org/10.1016/j.tws.2017.05.004
Received 13 November 2016; Received in revised form 2 May 2017; Accepted 4 May 2017
Available online 09 May 2017

plates and beams, and a satisfying accuracy was achieved [23–26]. In order to optimize the stiffener layout more effectively, many kinds of software are committed to this work. PANDA2 [27,28] can design composite stiffened shells under as many as five combined load cases based on gradient optimization algorithm. VICONOPT [29] is able to analyze the buckling and vibration problems of anisotropic plates. Furthermore, it can also optimize thin-wall structures under buckling constraints. Indeed, due to the introduction of NURBS [30,31] to describe the stiffener path, the computational cost of designing curved paths of stiffeners still face enormous challenges. Worse yet, in the design space, curvilinearly stiffened panels are always characterized by many local minima, which also increase the calculation burden remarkably. To solve this problem, more efficient global optimization algorithms and frameworks are crucial. The authors [32] proposed a novel stepwise design method to optimize cylindrical shells with curvilinear stiffeners. Mulani et al. [33,34] designed the stiffeners placement and size of stiffened panels by Response Surface Method (RSM), and the optimization process is decomposed into sizing optimization and stiffener placement optimization. Therefore, this approach is able to avoid trapping in local optimum and find global minima. In addition, dynamically reconfigurable quantum particle swarm optimization (PSO) was also used to find the optimal design of stiffened composite cylinders [35]. Compared with previous PSO algorithms, the quantum PSO can provide a more robust and reasonable optimal solution. It should be noted that above intelligence and genetic algorithms will cause much heavier computation burden compared to gradient-based optimization methods. In order to reduce the computational cost, a surrogate-based optimization framework with adaptive sampling was established by authors [36].

As a promising optimization technique, the HS algorithm was developed to search the optimum design of linear and nonlinear problems with both discrete and continuous variables [37]. This algorithm is in an analogy with music improvisation process where music players improvise the pitches of their instruments to obtain better harmony. During the improvisation process, all the solution vectors are stored in the harmony memory (HM), which is similar to the genetic pool in the genetic algorithm. In the HS algorithm, improvisation process continues to improve her/his contribution for a better state search of harmony [38,39]. The perfect harmony and improvisation group are corresponding to the global optimum and design variables, respectively. Originally, Geem et al. [40] developed the HS algorithm. Later, Mahdavi et al. [39] proposed the improved harmony search algorithm (IHS) whose parameters are dynamically updated at each iteration. Omran and Mahdavi [41] proposed the Global-best harmony search (GHS) algorithm based on a modified pitch adjustment rule where the best harmony is considered in new harmony memory. Kattan and Abdullah [37] extended the IHS based on the best-to worst harmony memory, adaptively. El-Abd [42] introduced an improved global-best harmony search (IGHS) algorithm and with a novel pitch generation scheme using the Gaussian and uniform distribution in the pitch process.

The structure of this paper is organized as below. In Section 2, the optimization method is introduced, including standard HS algorithm and a series of improved HS algorithm. On this basis, a modified version of HS algorithm (adaptive dynamic harmony search (ADHS) algorithm) is proposed based on the information of the harmony memory for improvisation procedure. In Section 3, the numerical model of curvilinearly stiffened shell is established. In order to reduce the amount of calculation, response surface method (RSM) is employed, and second-order polynomial with cross terms is used to construct the model. In Section 4, the optimum designs of aircraft panels are evaluated, and different harmony search algorithms are compared, and then the effects of the number of improvisation and harmony memory size are investigated.

2. Adaptive dynamic harmony search optimization

For the HS algorithm, there are five parameters including harmony memory size (*HMS*), harmony memory consideration rate (*HMCR*), pitch adjustment rate (*PAR*), bandwidth (*bw*) and number of improvisations (*NI*). In particular, *HMCR*, *bw* and *PAR* are the main parameters. In the improved versions of HS, some of these parameters are considered as a constant value or are computed dynamically using another parameter. To search the optimum of objective function, the sets of design variables are randomly generated based on those parameters, and five basic steps are included [40].

1) Define the optimization problem and parameters of the problem
2) Determine the initial values of the harmony memory
3) Create a new harmony memory
4) Update the harmony memory
5) Check the stopping criterion of the algorithm optimization: Terminate when the maximum number of improvisations is reached.

Based on the initial harmony memory in the second step, each generated member of the previous harmony memory are improvised using algorithm parameters such as *HMCR*, *PAR* and *bw*. This improvisation leads to a new harmony memory based on three rules: 1) consideration of the previous harmony memory members; 2) adjustment of the existing harmony memory; 3) random selection of each member of memory [43]. The parameter *HMCR* shows the selection rate of new memory from the previous harmony memory. The *PAR* is similar to the mutation of GA algorithm and adjusts the design variable of harmony memory randomly. Based on the randomness of improvisation in HS, the improvisation in harmony search optimization algorithms is introduced.

2.1. Harmony search

The memory consideration, pitch adjustment, and randomization are applied to improve new harmony for each design variable in the standard HS algorithm as follows:

Algorithm 1. The harmony search algorithm

IF $r_1 \le HMCR$ **then**
  $x_i'^j = x_i^j$; /select from previous harmony memory/
  IF $r_2 \le PAR$ **then**
    $x_i'^j = x_i^j + (2r-1) \times bw$; /adjust new harmony memory/
  ENDIF
ELSE
  $x_i'^j = x_i^L + r_3 \times (x_i^U - x_i^L)$; /select from the domain of variables/
ENDIF;
$F'^j = f(x'^j)$; /Computing the objective function based on new harmony memory/

where, r, r_1, r_2, $r_3 \in [0\ ,\ 1]$ are random numbers. $\boldsymbol{x}$ is the set of design variables, x_i^L and x_i^U are the upper and lower bounds of x_i respectively, which is the set of the possible range for each design variable. Hence, each design variable is placed in the domain $x_i \in [x_i^L, x_i^U]$.

2.2. Improved harmony search

The parameters of improved harmony search (IHS) including *PAR* and *bw* are dynamically updated during the evolution by the following equations [39]:

$$PAR(k) = PAR_{\min} + \frac{PAR_{\max} - PAR_{\min}}{NI}k \quad (1)$$

$$bw(k) = bw_{\max}\exp[\frac{Ln(bw_{\min}) - Ln(bw_{\max})}{NI}k] \quad (2)$$

where, $PAR_{\min}$ and $PAR_{\max}$ are the minimum and maximum values of the pitch adjusting rate, respectively. $PAR(k)$ is the calculated pitch adjusting rate for the kth generation. In Eq. (2), $bw_{\min}$ and $bw_{\max}$ are the minimum and maximum values of the distance bandwidth respectively, and $bw(k)$ is the obtained distance bandwidth for the kth generation. The IHS is the same as the basic HS algorithm, but exhibits better performance for optimization problems [39,42]. Therefore, adjusting step for improvisation of the IHS algorithm is shown as follows:

Algorithm 2. The improved harmony search algorithm

IF $r_1 \le HMCR$ **then**
  $x_i'^j = x_i^j$; /select from previous harmony memory/
  IF $r_2 \le PAR(k)$ **then**
    $x_i'^j = x_i^j + (2r-1)\times bw(k)$; /adjust new harmony memory based on dynamical bandwidth Eq. (2)/
  ENDIF
ELSE
  $x_i'^j = x_i^L + r_3\times(x_i^U - x_i^L)$; /select from the domain of variables/
ENDIF;
$F'^j = f(x'^j)$; /compute the objective function based on new harmony memory/

2.3. Global-best harmony search

Mahdavi and Omran [41] proposed the GHS based on the best harmony in the harmony memory. The pitch adjustment step of the HS is modified by the best harmony. Additionally, the parameter PAR is determined by a dynamic updating procedure based on Eq. (1). The improvisation step of the GHS is similar to the basic HS algorithm, but the improvisation step of GHS is modified as follows:

Algorithm 3. global-best harmony search algorithm

IF $r_1 \le HMCR$ **then**
  $x_i'^j = x_i^j$; /select from previous harmony memory/
  IF $r_2 \le PAR(k)$ **then**
    $x_i'^j = x_i^{best}$; /adjust new harmony memory based on the best harmony in memory/
  ENDIF
ELSE
  $x_i'^j = x_i^L + r_3\times(x_i^U - x_i^L)$; /select from the domain of variables/
ENDIF;
$F'^j = f(x'^j)$; /compute the objective function based on new harmony memory/

where, x_i^{best} means the best harmony of the i_{th} design variable in the memory. $PAR(k)$ is the dynamical pitch adjusting rate for the k_{th} generation, which is computed by Eq. (1).

2.4. Improved global best harmony search

An improved version of global-best harmony search algorithm was introduced by El-Abd [42] that has better efficiency and performance than the HS algorithm. The harmony memory with probability of $HMCR$ is adjusted using random generation based on standard normal probability distribution. Then, the best harmony is adjusted using the uniform distribution and the bandwidth, which was developed by Mahdavi et al. [39] in Eq. (2). The adjusting step of new harmony memory for IGHS algorithm is shown as follows:

Algorithm 4. improved global -best harmony search algorithm

IF $r_1 \le HMCR$ **then**
  $x_i'^j = x_i^j + Gr(0,\ 1)\times bw(k)$; /adjust the HM using the Gaussian standard distribution/
  IF $r_2 \le PAR(k)$ **then**
    $x_i'^j = x_i^{best} + (2r-1)\times bw(k)$; /adjust the new HM with the best memory by bw (proposed by Mahdavi *et al.* (2007))/
  ENDIF ELSE
    $x_i'^j = x_i^L + r_3\times(x_i^U - x_i^L)$; /select from the domain of variables/
ENDIF
$F'^j = f(x'^j)$; /compute the objective function based on new harmony memory/

in which, $Gr(0,\ 1)$ is a random number generated using Gaussian standard distribution with a mean of 0 and a standard deviation of 1. The pitch adjusting rate (PAR) and bandwidth (bw) are dynamically calculated by Eqs. (1) and (2) in IGHS algorithm.

2.5. Adaptive dynamic harmony search

In this study, a modified version of HS algorithm is proposed based on the information of the harmony memory for improvisation procedure. The new harmony memory is dynamically determined based on two adjusting stages in the adaptive dynamic harmony search (ADHS) algorithm. In the first stage, the harmony memory is adjusted using the maximum and minimum numbers of each design variable in HM with a dynamical HMCR as follows:

$$HMCR(k) = 0.95 + 0.1\times\sqrt{\frac{k}{NI} - (\frac{k}{NI})^2} \quad (3)$$

where k is the number of the current iteration, NI is the total number of iterations. Therefore, the new harmony memory based on $HMCR$ (k) in Eq. (3) is computed as

$$x_i'^j = \begin{cases} x_i'^j \pm \sqrt{1 - k/NI}\times Bw_i(k) & \text{with probability } HMCR\ (k) \\ x_i^L + r\times(x_i^U - x_i^L) & \text{with probability } 1{-}HMCR\ (k) \end{cases} \quad (4)$$

where, $Bw(k)$ is a dynamical bandwidth, which is suggested as follows:

$$Bw_i(k) = \frac{x_i^{\max} - x_i^{\min} + 0.001}{10}\exp[-10\frac{k}{NI}] \quad (5)$$

where $x_i^{\max}$ and $x_i^{\min}$ are the maximum and minimum values for design variable x_i in HM, respectively. According to Eq. (5), a bandwidth is developed based on a mathematical function using the maximum and minimum harmony memory for each iteration. The proposed bandwidth is larger at the initial iterations, because a maximum difference is obtained between $x_i^{\max}$ and $x_i^{\min}$. Consequently, a larger bandwidth is considered to adjust the harmony in ADHS. The dynamical bandwidth is decreased based on the increment of improvisation as logarithmic (bandwidth is about $Bw_i(NI) \approx 4.54\times10^{-6}(x_i^{\max} - x_i^{\min})$ at the end of iterations), and the difference between the maximum and minimum harmony memory is decreased in successive iterations. Therefore, the bandwidth is reduced at the final iterations. The dynamical bandwidth is established based on the number of current improvisation, minimum and maximum values of each design variable in the harmony memory.

In the second stage, the new HM is adjusted using the coefficient $\sqrt{1-k/NI}$ and the dynamic pitch adjustment rate (PAR (k)) by the following relations:

$$PAR(k) = 0.3 + 0.6 \times [1 - \sqrt{1-k/NI}] \tag{6}$$

$$x_i'^j = \begin{cases} x_i^j \pm \sqrt{1-\frac{k}{NI}} \times [x_i^{\max} - x_i^{\min}] & \text{with probability } PAR(k) \\ x_i^L + r \times (x_i^U - x_i^L) & \text{with probability } 1-PAR(k) \end{cases} \tag{7}$$

As can be seen from Eqs. (6) and (7), each element in harmony memory is adapted with an interval $[x_i^{\min}, x_i^{\max}]$ at each iteration. This line search direction (i.e. $x_i^{\max} - x_i^{\min}$) for each variable is used to move each harmony memory corresponding to the maximum and minimum harmony memory. Generally, a global adjustment is achieved based on the proposed adjustment processes in the second stage, where the movement of each harmony from the previous position is controlled by the coefficient $\sqrt{1-k/NI}$. The value of $\sqrt{1-k/NI}$ is determined as a smaller value at the final iteration, thus the new HM is adapted with a smaller bandwidth i.e. $\sqrt{1-k/NI} \times [x_i^{\max} - x_i^{\min}]$. On the other hand, the proposed line search to adapt the HM in the first stage is obtained as a larger value at the initial iterations in order to determine a larger $\sqrt{1-k/NI}$ and larger difference between the maximum and minimum values for design variable x_i, thus a wide area for searching the pitch adjustment of each design variable is randomly selected.

As is evident, the harmony memory is adjusted with the probability of $HMCR \times PAR$ based on a dynamical pitch adjustment with a bandwidth in Eq. (7). This dynamical bandwidth can adjust the new HM in local position of each design variable. Therefore, the local optimum solutions may be reduced based on the ADHS for optimization problems with several local minima. The ADHS to determine the optimum condition is defined based on the following steps, which can be implemented in a computer program to optimize complex engineering problems.

Algorithm 5. adaptive dynamic harmony search algorithm

Step 1: **DEFINE** HMS, $X \in [X^L, X^U]$, $k=1$;

Step 2: **FOR** j←1 to MHS **DO**

FOR i←1 to N **DO** /for number of design variables (N)/

$x_i^j = x_i^L + r \times (x_i^U - x_i^L)$; in which $r \in [0, 1]$

END FOR

$F^j = f(\boldsymbol{X}^j)$ / objective function at the harmony memory $\boldsymbol{X}^j$/

END FOR

Step 3: **FOR** i←1 to N **DO**

Find the maximum harmony ($x_i^{\max}$) and minimum harmony ($x_i^{\min}$) for variable x_i

Compute the parameters of ADHS as

$\gamma(k) = \sqrt{1-k/NI}$ **and**

$L_i = x_i^{\max} - x_i^{\min}$

$Bw_i(k) = \frac{L_i + 0.001}{10} \exp[-10\frac{k}{NI}]$,

$PAR(k) = 0.3 + 0.6 \times [1 - \gamma(k)]$,

$HMCR(k) = 0.95 + 0.1 \times \sqrt{\gamma(k)}\sqrt{k/NI}$

FOR j←1 to MHS **DO**

IF $r_1 \le HMCR(k)$ **THEN** in which $r_1 \in [0, 1]$

$x_i'^j = x_i'^j \pm \gamma(k) \times Bw_i(k)$; /pitch the harmony memory in terms of local position/

IF $r_2 \le PAR(k)$ **THEN** in which $r_2 \in [0, 1]$ /pitch the new harmony memory as global position/

$x_i'^j = x_i^j \pm \gamma(k) \times L_i$

ENDIF ELSE

$x_i'^j = x_i^L + r \times (x_i^U - x_i^L)$; in which $r \in [0, 1]$ /select the new HM from the domain of design variables/

ENDIF

END FORs

Step 4: **FOR** j←1 to MHS **DO**

$F'^j = f(\boldsymbol{X}'^j)$ / objective function at the new harmony memory $\boldsymbol{X}'^j$/

IF $F'^j < F^j$ **THEN** $\boldsymbol{X}^j = \boldsymbol{X}'^j$ **END IF**

END FOR

Step 5: **IF** k=**NI AND** F^j ***satisfies the convergence criteria*** **THEN** ***report results and*** **STOP**

ELSE $k=k+1$ and return to Step 3

END IF

---

3. Numerical example

3.1. Model description

A curvilinearly stiffened panel with multiple cutouts for aircraft design is established in this section, which was designed, manufactured and tested in the Combined Load Test Fixture at NASA Langley Research Center by Havens et al. [44]. This stiffened panel is representative of a large wing engine pylon rib, with a length of $L=711.2$ mm, a width of $B=609.6$ mm, as shown in Fig. 1. There are four curvilinear stiffeners and two circular cutouts, and both of the cutouts are reinforced by thick circular ring area. Unlike the work by Havens et al. [44], only axial compression is considered in this paper. The thickness of two thick circular reinforced rings are 5.9 mm and 4.7 mm, respectively. All stiffeners have same thickness and height. The stiffener height h is 13.4 mm, and the thickness t is 1.6 mm. The skin thickness t_c is 2.6 mm. The aluminum alloy 2139 is used to manufacture this shell, with the material properties listed as follows: Young's modulus $E=72504$ MPa, Poisson's ratio $\upsilon=0.33$, density $\rho=2.8E\text{-}6$ kg/mm^3 and yield stress $\sigma_s=465.8$ MPa. The structural weight of the initial design is 3.27 kg.

To prevent the distortion along shell edge and thus virtual buckling modes, all the loading-end nodes are coupled to a central reference point with a rigid body link to enforce a uniform displacement condition, and two sides are simply supported. There are three variables (cover thickness t_c, stiffener thickness t, stiffener height h) in this model, which follow normal distribution. By performing the linear buckling analysis in FE package ABAQUS, the predicted buckling load is 38.3 kN, and the first buckling mode shape is shown in Fig. 2.

3.2. Response surface method for performance prediction

Buckling analysis is relatively time-consuming for global optimization. Originally, the response surface method (RSM) is an appropriate tool to calibrate the mathematical model-based polynomial functions for estimation of mechanical experiments, which approximates an implicit or complex process as a response surface function (RSF) in an explicit and simple polynomial form based on evaluation of the experimental points of a mechanical event. The second-order polynomial form can be used to reassert the RSF, and the second-order polynomial form of RSF with cross terms is expressed as [45,46].

$$f(X) = a_0 + \sum_{i=1}^{n} a_i x_i + \sum_{i=1}^{n} a_{ii} x_i^2 + \sum_{i=1}^{n} \sum_{j=i+1}^{n} a_{ij} x_i x_j \tag{8}$$

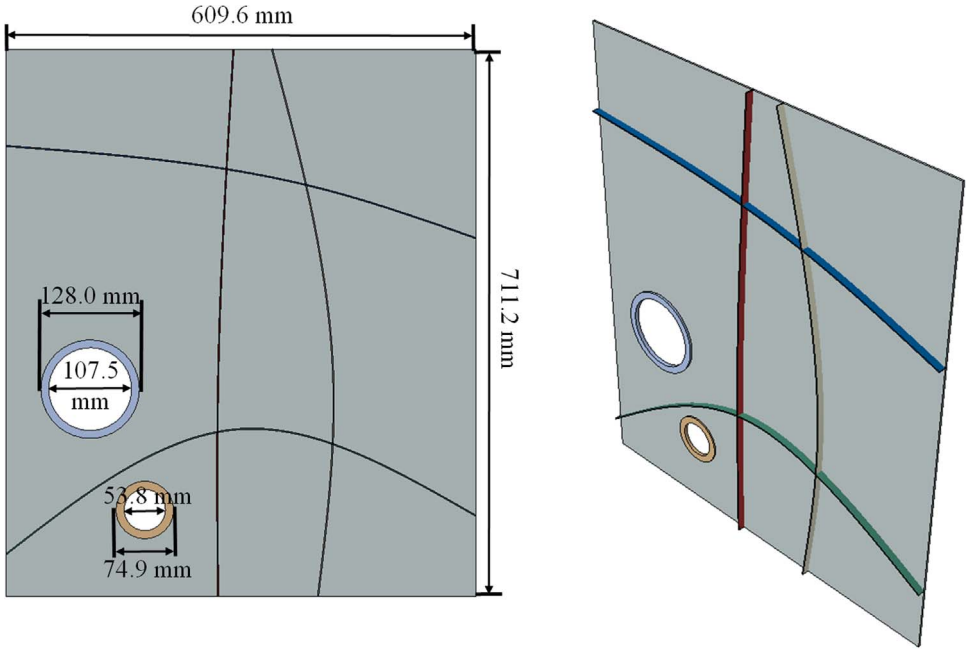

Fig. 1. Sketch of the curvilinearly stiffened panel with multiple cutouts.

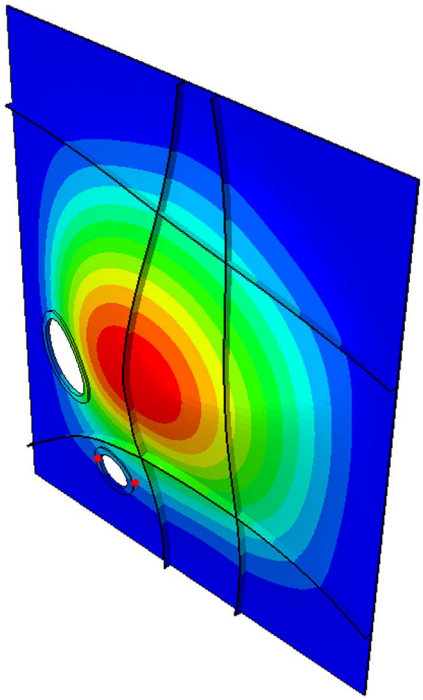

Fig. 2. First buckling mode shape of the initial design.

where, a_0, a_i, a_{ii} and a_{ij} are the unknown coefficients, and the number of coefficients necessary to define is $(n+1)(n+2)/2$. The accuracy of predicting the mechanical properties may be improved through the inclusion of the cross terms in the second-order polynomial RSF. The least squares estimator commonly used in evaluating the unknown coefficients of the RSF in terms of the experiment data points [46,47]. The main goal in the RSM is to fit a RSF to the experiment points. The approximated RSF can be rewritten in matrix form as follows:

$$f(\boldsymbol{X}_i) = P(\boldsymbol{X}_i)^T \boldsymbol{a} \tag{9}$$

where $f(\boldsymbol{X}_i)$ is the prediction value based on experimental input data $\boldsymbol{X}$. $\boldsymbol{a}$ is the coefficient vector, which can be computed based on variables $\boldsymbol{X}$ at each experiment for mechanical properties. $P(\boldsymbol{X}_i)$ is the polynomial basic function vector at the observed data points $\boldsymbol{X}_i$, and the basic functions for second-order polynomial of RSF with three input variables is defined as

$$P(\boldsymbol{X}) = [1,\ x_1,\ x_2,\ x_3,\ x_1^2,\ x_2^2,\ x_3^2,\ x_1x_2,\ x_1x_3,\ x_2x_3] \tag{10}$$

The unknown coefficient $\boldsymbol{a}$ is computed by minimizing the error between the observed (O) and approximation ($f(\boldsymbol{X})$) data. The error is determined by the following relation:

$$e(\boldsymbol{X}_i) = \sum_{i=1}^{NE} [O_i - f(\boldsymbol{X}_i)]^2 = \sum_{i=1}^{NE} [O_i - P(\boldsymbol{X}_i)^T \boldsymbol{a}]^2 \tag{11}$$

where, NE is the number of data points in $\boldsymbol{O} = [O_1,\ O_2,\ O_3,\ ...O_{NE}]^T$ and $P(\boldsymbol{X})^T = [P(X_1),\ P(X_2),\ P(X_3),\ ...P(X_{NE})]$. By minimizing the error function in Eq. (11) with respect to the unknown coefficient $\boldsymbol{a}$, we have

$$\boldsymbol{a} = [P(\boldsymbol{X})^T P(\boldsymbol{X})]^{-1} [P(\boldsymbol{X})^T \boldsymbol{O}] \tag{12}$$

In this way, the surrogate model-based RSF is determined, more simply. The weight and the buckling load of aircraft panels can be estimated by the second-order RSF.

The response surface function in Eq. (8) is calibrated based on data points. The unknown parameters for second-order polynomial function of weight and buckling load are determined based on Eq. (12) with input variables; t, t_c and h in this study.

3.3. Comparative studies of the input variables

The observed and predicted values from the RSF for weight (W) and buckling load (P_{cr}) are plotted in Fig. 3a and b, respectively. As can be seen, the RSFs, which can be used to prediction of W and P_{cr}, have a good performance, since the predictions are close to the experiment data point. The root mean square errors (RMSE) and adjusted correlation (R^2) are computed for the RSFs as RMSE = 0.003 kg and $R^2 = 1$ for W, RMSE = 0.75762 kN and $R^2 = 0.997$ for P_{cr}. Consequently, the RSF can be used for the optimization and evaluation of the optimum condition based on the proposed ADHS.

Firstly, the weight and buckling load of aircraft panels are evaluated based on the second-order RSF with cross terms. The effects of three design variables (i.e. cover thickness t_c, stiffener height h and thickness t) are investigated with regard to the initial design $(t_c,\ h,\ t)_{\text{int}} =$ (2.6 mm, 13.4 mm, 1.8 mm). The initial weight and buckling load are

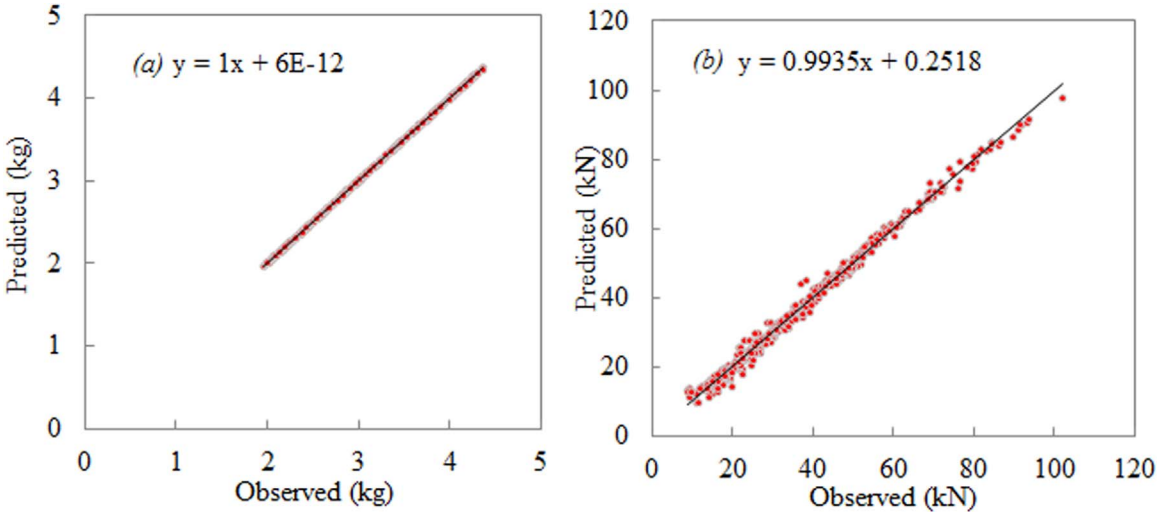

Fig. 3. The observed experiments and predicted RSF for weight and buckling load of aircraft panels. (a) weight (kg); (b) buckling load (kN).

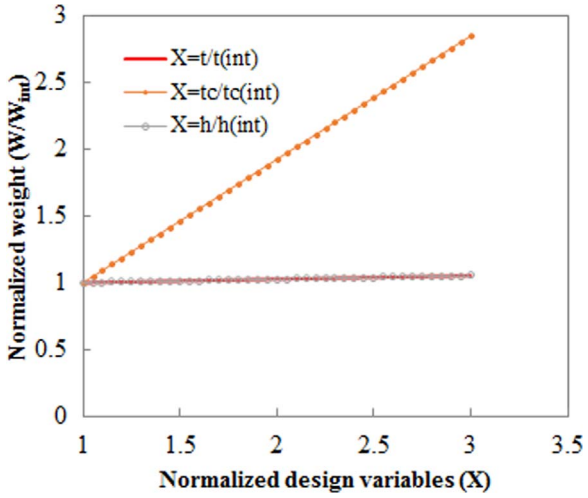

Fig. 4. The effects of design variables on the weight of aircraft panels.

estimated for the initial design using RSM as $W_{int}=3.2889$ kg and $P_{cr\ int}=40.3825$ kN, respectively. The normalized weight (weight to initial weight i.e. W/W_{int}) with respect to the normalized design variables is plotted in Fig. 4. It can be seen from Fig. 4 that the weight is more sensitive to skin thickness than other design variables i.e. *h,* and *t.*

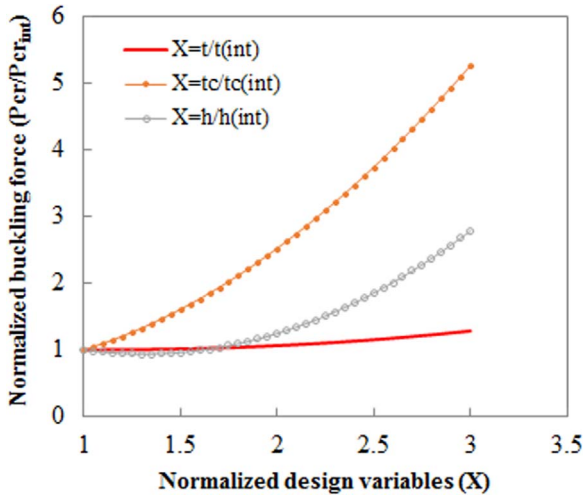

Fig. 5. The effects of design variables on the buckling load of aircraft panels.

Fig. 5 illustrates the normalized buckling load (buckling load to initial buckling load i.e. $P_{cr}/P_{cr\ int}$) with respect to the normalized design variables. As expected, the buckling load is increased by increasing the design variables. The buckling load is increased about 5.26, 2.67 and 1.27 times when the normalized variables (i.e. skin thickness t_c, stiffener height h and thickness t) are increased to 3, respectively. In addition, it can be found that the effect of skin thickness t_c is more than other design variables i.e. h and t. However, the buckling load with respect to stiffener height (h) is more sensitive than stiffener thickness t but this variable h is not shown a significant weight difference between panels with a same $t_c=1.5$ mm and $t=0.8$ mm, and different stiffener heights 8 mm and 24 mm.

4. Comparative results and discussion

In this section, two applications of the optimization approach using response surface method and proposed ADHS method are discussed. In the first application, the optimum designs of aircraft panels based on different harmony search algorithms are evaluated and the results are compared, and then, in the second application, the optimum designs based on the proposed ADHS algorithm are evaluated with respect to various constraints of buckling load, stiffener height and thickness. The optimization model to search the optimum conditions of the aircraft panels is given as follows:

$$\begin{aligned} &find \quad t_c^*,\ h^*,\ t^* \\ &\min \quad W=f(t_c,\ h,\ t) \\ &S.\ t. \quad P(t_c,\ h,\ t)\geq P_{cr} \\ &\qquad 0.5\leq t_c\leq 3.75cm,\ \ 8\leq h\leq 18cm,\ \ 0.5\leq t\leq 2.5cm \end{aligned} \tag{13}$$

where, t_c^*, h^* and t^* are the optimum design variables. W and $P(t_c,\ h,\ t)$ are the weight and buckling load of aircraft panels respectively, which are predicted at the design point (t_c, h, t) based on the RSF with cross terms. P_{cr} is the buckling load constraint. To evaluate the ability to search the optimum design, an unconstrained optimization function is used by the penalty functions as $F=W+\lambda[g(t_c,\ h,\ t)]^{\eta}$, in which λ and η are the penalty coefficients as $\lambda=10^4$ and $\eta=2$. $g(t_c,\ h,\ t)$ is the penalty function, which is determined by $g(t_c,\ h,\ t)=\max\{0,\ P_{cr}-P(t_c,\ h,\ t)\}$.

4.1. Comparison of different harmony search algorithms

In this section, five harmony algorithms with a same number of improvisation i.e. $NI=5000$ and harmony memory size i.e. $HMS=5$ [42] are compared. To be specific, the parameters are considered as $HMCR=0.95$ for all algorithms; $bw=(x_{max}-x_{min})/100$, and $PAR=0.35$

Table 1
Results of different harmony search algorithms for aircraft panels.

Method	HS	IHS	GHS	IGHS	Proposed ADHS
W (mean) (kg)	3.4740	3.3963	3.4428	3.4963	2.8449
SD (kg)	0.3698	0.4085	0.4273	0.3891	0.1232
W (best) (kg)	2.8289	2.7468	2.7983	2.7603	2.7265
Optimum variable value					
t_c^* *(mm)*	2.0762	1.9948	2.0358	2.0164	1.9598
h(mm)*	17.1331	18.00	17.2952	18.00	18.00
t(mm)*	2.3772	2.3544	2.4774	2.2707	2.50
ABAQUS (*W*)	2.8289	2.7468	2.7983	2.7603	2.7265
ABAQUS (P_{cr})	44.812	40.558	42.933	41.471	39.148
Rel-errors (*W*) %	−9.48E−06	−1.23E−05	−1.46E−05	−9.02E−06	−1.90E−05
Rel-errors (P_{cr}) %	−14.53	−5.57	−10.79	−7.65	−2.17

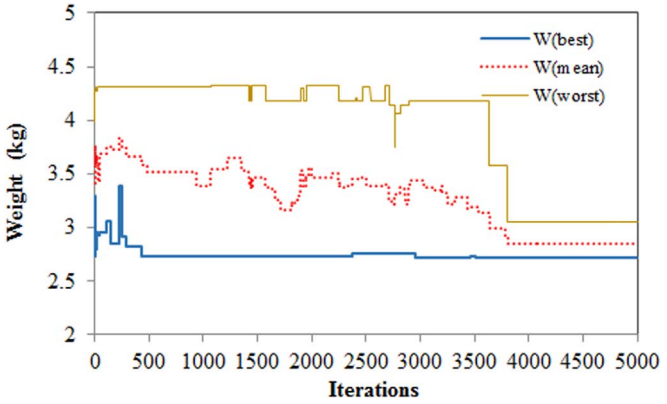

Fig. 6. Iterative histories of optimum weight for ADHS with *HMS* = 5.

for HS algorithm; $bw_{max} = (x_{max} - x_{min})/20$, $bw_{min} = 0.001$, $PAR_{max} = 0.9$, $PAR_{min} = 0.1$ for IHS and IGHS [42]; $PAR_{max} = 0.9$, $PAR_{min} = 0.1$ for GHS. The parameters of harmony search method based on the adaptive dynamical algorithm are dynamically determined at each iteration. The optimum designs of this complex problem, which is described in Section 3.1, are obtained based on the HS, IHS, GHS, IGHS, ADHS respectively, and the corresponding results are listed in Table 1. The optimum weight is obtained based on 30-run iterations for each algorithm, and then the average value i.e. *W* (mean), standard deviations SD and best solution (minimum weight) i.e. *W* (best) as well as the optimum variable values are tabulated in Table 1. Also, the average *W* (mean), best *W* (best) and worst *W* (worst) solutions in 30-runs for each iteration are plotted in Fig. 6 for the proposed ADHS algorithm. The results in Table 1 demonstrate that the harmony search algorithms can be used to search the optimum designs of this complex example, successfully. In addition, it can be found that the IGHS algorithm has a better performance than the HS, IHS, and GHS, but the proposed method obtains a superior optimum design than the IGHS i.e. *W* (best) = 2.2027 kg. The HS and GHS yield maximum average and best solutions among other harmony algorithms. The results from Fig. 6 and Table 1 show that the difference between the average optimum weight of the proposed ADHS and the best solution is about 0.23 kg, but the corresponding values are obtained as 1.034 kg for HS, 0.37 kg for IHS, 0.667 kg for GHS and 0.904 kg for IGHS. This means that the proposed ADHS can provide an optimum design in a robust manner when compared with other harmony algorithms. In the ADHS, the dynamic pith stage based on the novel generated harmony memory produces an appropriate optimum design. The optimum variable values based on the ADHS are obtained as (t_c^*, h^*, t^*) = (1.703789 mm, 18 mm, 2.5 mm) with an optimal weight of 2.4281 kg. As can be seen, both h^* and t^* are converged to the upper bounds. Therefore, the geometrical dimensions of stiffener are the important factors to balance improved load-carrying capacity and optimum weight of aircraft panels.

Table 2
Effects of *NI* on the optimum design using different harmony search algorithms.

Method		HS	IHS	GHS	IGHS	ADHS
NI = 50	*W* (mean) (kg)	3.5785	3.5638	3.4527	3.6746	3.2714
	SD (kg)	0.4002	0.3717	0.3933	0.4127	0.4591
	W (best)(kg)	2.9193	2.8091	2.8941	2.8934	2.7278
NI = 100	*W* (mean) (kg)	3.6461	3.4547	3.3564	3.5125	3.3391
	SD (kg)	0.3838	0.4382	0.4083	0.4564	0.4610
	W (best)(kg)	2.9378	**2.7381**	2.8267	2.8537	2.7272
NI = 500	*W* (mean) (kg)	3.6333	3.5621	3.4987	3.4988	3.1319
	SD (kg)	0.4202	0.3299	0.3625	0.3858	0.3639
	W (best)(kg)	**2.8448**	2.7945	2.8766	2.9079	2.7272
NI = 1000	*W* (mean) (kg)	3.5547	3.3633	3.5514	3.6477	2.9276
	SD (kg)	0.4283	0.4692	0.4182	0.4337	0.2635
	W (best)(kg)	2.9004	2.7382	2.8528	**2.7465**	2.7266
NI = 2000	*W* (mean) (kg)	3.3803	3.5584	3.4570	3.5095	2.8926
	SD (kg)	0.3414	0.3531	0.3822	0.3749	0.1813
	W (best)(kg)	2.8803	2.9621	**2.8058**	2.9396	**2.7265**

*The bold numbers are the best optimum results among different NI for each algorithm.

4.2. Effects of the number of improvisation

The number of improvisation (*NI*) is one of important parameters in ADHS based on Eqs. (3)–(7), since most of ADHS parameters are dynamically evaluated by *NI*. Thus, the effects of *NI* are investigated based on the optimum designs using different harmony search algorithms. The statistical results including mean, SD and best solutions for the optimum weight of aircraft panels are tabulated in Table 2 for HS, IHS, GH, IGHS and proposed ADHS methods. The iterative histories for the proposed ADHS algorithm with different *NI* are shown in Fig. 7. The results in Table 2 indicate that the means of optimum weight can be decreased by increasing the *NI* for the proposed ADHS (*W* (mean)

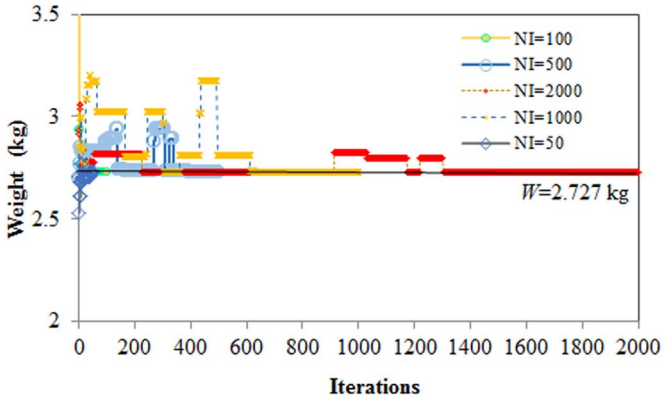

Fig. 7. Iterative results of optimum weight for different numbers of improvisation (*NI*) in ADHS algorithm.

Table 3
Effects of *HMS* on the optimum design using different harmony search algorithms.

Method		HS	IHS	GHS	IGHS	ADHS
HMS = 5	*W* (mean) (kg)	3.3803	3.5584	3.4570	3.5095	2.8926
	SD (kg)	0.3414	0.3531	0.3822	0.3749	0.1813
	W (best)(kg)	2.8803	2.9621	2.8058	2.9396	2.7265
HMS = 10	*W* (mean) (kg)	3.3693	3.2930	**3.4032**	3.4115	2.8054
	SD (kg)	0.3234	0.3294	**0.3680**	0.3118	0.1282
	W (best)(kg)	2.8165	2.7707	**2.7922**	2.8789	2.7265
HMS = 20	*W* (mean) (kg)	3.3533	3.2387	3.4721	3.5129	2.7587
	SD (kg)	0.3831	0.3302	0.3945	0.4504	0.0578
	W (best)(kg)	2.8539	2.7566	2.8575	2.7305	2.7236
HMS = 30	*W* (mean) (kg)	3.2386	**2.9542**	3.5907	**3.4757**	2.7236
	SD (kg)	0.3404	**0.1978**	0.4427	**0.4314**	0.0050
	W (best)(kg)	2.7700	**2.7355**	2.8323	**2.7293**	2.7147
HMS = 50	*W* (mean) (kg)	**3.0522**	3.0360	3.5205	3.4561	**2.7150**
	SD (kg)	**0.2325**	0.2407	0.4083	0.4331	**0.0005**
	W (best)(kg)	**2.7400**	2.7371	2.8881	2.7875	**2.7147**

*The bold numbers are the best optimum results among different HMS for each algorithm.

= 3.27 kg at *NI* = 50 and *W* (mean) = 2.89 kg at *NI* = 2000), however, the best solution is almost unchanged for *NI* = 50 and *NI* = 2000 i.e. $W_{best} \approx 2.726$ kg (see Fig. 7). By contrast, the IGHS, GHS, IHS as well as HS methods exhibit different performances when increasing the *NI*, specifically, *W* (best) = 2.845 kg at *NI* = 500 for HS, *W* (best) = 2.738 kg at *NI* = 100 for IHS, *W* (best) = 2.806 kg at *NI* = 2000 for GHS and *W* (best) = 2.747 kg at *NI* = 1000 for IGHS. On the other hand, the differences between the maximum and minimum values of best weight for various *NI* in the IGHS, GHS, IHS and HS algorithms are larger than the proposed ADHS. The proposed pith adjusted process based on a local and global adjusting formula with probability dynamical *HMCR* and *PAR*. Therefore, the proposed ADHS algorithm can provide an optimum result compared to other harmony algorithms based on a less harmony memory size (*HMS* = 5) and *NI* > 500 for this example, more efficiently.

4.3. Effects of the harmony memory size

In the studied HS methods, *HMS* determines the scale of initial solution, and its value will influence the efficiency and accuracy of HS algorithms. A larger *HMS* means that the algorithm has a higher chance to find a better feasible solution. In this section, the effects of the harmony memory size are discussed between HS, HIS, GHS, IGHS and ADHS. As the statistical results of the optimum weight of aircraft panels are listed in Table 3, *W* (best) = 2.74 kg at *HMS* = 50 for HS, *W* (best) = 2.7355 kg at *HMS* = 30 for IHS, *W* (best) = 2.7922 kg at *HMS* = 10 for GHS, *W* (best) = 2.7293 kg at *HMS* = 30 for IGHS and *W* (best) = 2.7147 kg at *HMS* = 50 for IGHS. Along with an increasing value of *HMS*, most of HS algorithms obtain a better result for both the mean and best of solution. However, with the increase of *HMS*, GHS obtains the best solution at *HMS* = 10, and *W* (best) at *HMS* = 5 and *HMS* = 20 are also superior to the solution at *HMS* = 50. The means and best of optimum weight can be decreased by increasing the *HMS* for the proposed ADHS (*W* (mean) = 2.8926 kg, *W* (best) = 2.7265 kg at *HMS* = 5 and *W* (mean) = 2.715 kg, *W* (best) = 2.7147 kg at *HMS* = 50). It should be noted that the *W* (mean) and *W* (best) of ADHS at *HMS* = 5 is even better than *W* (mean) and *W* (best) of HS, IHS, GHS and IGHS at *HMS* = 50. It means that ADHS can achieve a better performance than HS, IHS, GHS and IGHS with a smaller amount of calculation. From Table 3, the ADHS gets the smallest value of SD at each *HMS*, even at *HMS* = 5, the divergence of solution is better than other algorithms at *HMS* = 50. In particular, when *HMS* = 50, SD = 0.0005, which indicates the HM converges to a stable solution. The harmony memory of ADHS is adjusted with the probability of *HMCR* × *PAR* based on a dynamical pitch adjustment with dynamical bandwidth, which can adjust the new HM in local position of each design variable. Therefore, local optimum solutions may be reduced based on the ADHS for optimization problems with multiple local minima, which will make the algorithm more robust and efficient.

5. Conclusions

Structural weight is crucial for aircraft panels under buckling constraint, and thus the minimum-weight optimization is of great concerns. In this study, a modified version of HS algorithm is proposed based on the information of the harmony memory to find the optimum design of aircraft panels, named as adaptive dynamic harmony search (ADHS) algorithm. Typical curvilinear stiffened panels under buckling constraint are considered, in order to demonstrate the advantage of the proposed algorithm. Based on the illustrative example, several existing harmony search algorithms are compared with the proposed algorithm, including the best solution, mean value and standard deviation of optimum results. Results indicate that the proposed ADHS can provide an optimum design in a robust manner. However, due to the inherence of evolutionary algorithm, the proposed method is still not suitable for super-dimensional problems. Therefore, the number of design variables should not be too large, otherwise, the global optimum design cannot be guaranteed.

Furthermore, the effects of the number of improvisation (*NI*) and harmony memory size (*HMS*) are investigated and discussed in detail. It is found that the differences between the maximum and minimum values of best weight for various *NI* in the IGHS, GHS, IHS and HS algorithms are larger than the proposed ADHS. Also, local optimum solutions may be reduced based on the ADHS for optimization problems with multiple local minima, which makes the algorithm more robust and efficient optimum results as $W^* = 2.7147$ kg with optimum conditions as skin thickness $t_c^* = 1.9497$ mm, stiffener thickness $t^* = 2.5$ mm, and stiffener height $h^* = 18$ mm.

Acknowledgements

This work was supported by the National Natural Science Foundation of China (11402049) and International Joint Research Project by University of Zabol (IR-UOZ96-8).

References

[1] M.W. Hilburger, V.O. Britt, M.P. Nemeth, Buckling behavior of compression-loaded quasi-isotropic curved panels with a circular cutout, Int. J. Solids Struct. 38 (2001) 1495–1522.
[2] J. Huang, R. Haftka, Optimization of fiber orientations near a hole for increased load-carrying capacity of composite laminates, Struct. Multidiscip. Optim. 30 (2005) 335–341.
[3] R. Degenhardt, S.G.P. Castro, M.A. Arbelo, et al., Future structural stability design for composite space and airframe structures, Thin-Walled Struct. 81 (2014) 29–38.
[4] R. Khakimova, R. Zimmermann, D. Wilckens, et al., Buckling of axially compressed CFRP truncated cones with additional lateral load: experimental and numerical investigation, Compos. Struct. 157 (2016) 436–447.
[5] P. Hao, B. Wang, K. Tian, et al., Integrated optimization of hybrid-stiffness stiffened shells based on sub-panel elements, Thin-Walled Struct. 103 (2016) 171–182.
[6] P. Hao, B. Wang, K. Tian, et al., Optimization of curvilinearly stiffened panels with single cutout concerning the collapse load, Int. J. Struct. Stab. Dyn. 16 (7) (2016) 1550036 (21 pages).
[7] G. Soni, R. Singh, M. Mitra, Buckling behavior of composite laminates (with and without cutouts) subjected to nonuniform in-plane loads, Int. J. Struct. Stab. Dyn. 13 (2013) 987–992.
[8] M. Shariati, M.M. Rokhi, Buckling of steel cylindrical shells with an elliptical cutout, Int. J. Steel Struct. 10 (2010) 193–205.
[9] A.L. Schlack Jr, Experimental critical loads for perforated square plates, Exp. Mech. 8 (1968) 69–74.
[10] R. Tennyson, The effects of unreinforced circular cutouts on the buckling of circular cylindrical shells under axial compression, J. Eng. Ind. 90 (1968) 541–546.
[11] J.M. Rotter, The new framework for shell buckling design and the european shell buckling recommendations fifth edition, J. Press. Vessel Technol. 133 (2010) (011203-011203).
[12] A. Tafreshi, Buckling and post-buckling analysis of composite cylindrical shells with cutouts subjected to internal pressure and axial compression loads, Int. J. Press. Vessels Pip. 79 (2002) 351–359.

[13] D. Schillinger, V. Papadopoulos, M. Bischoff, M. Papadrakakis, Buckling analysis of imperfect I-section beam-columns with stochastic shell finite elements, Comput. Mech. 46 (2010) 495–510.
[14] M.W. Hilburger, J.H. Starnes Jr, Buckling behavior of compression-loaded composite cylindrical shells with reinforced cutouts, Int. J. Non-Linear Mech. 40 (2005) 1005–1021.
[15] S.J. Guo, Stress concentration and buckling behaviour of shear loaded composite panels with reinforced cutouts, Compos. Struct. 80 (2007) 1–9.
[16] J. Cervantes, A.N. Palazotto, Cutout reinforcement of stiffened cylindrical shells, J. Aircr. 16 (1979) 203–208.
[17] P. Hao, B. Wang, G. Li, Z. Meng, K. Tian, D. Zeng, X. Tang, Worst Multiple Perturbation Load Approach of stiffened shells with and without cutouts for improved knockdown factors, Thin-Walled Struct. 82 (2014) 321–330.
[18] B.M. Madhura, Damage tolerance evaluation of wing in presence of large landing gear cutout through stress analysis using FEM, Ijrset Org. (2014).
[19] R. Kapania, J. Li, H. Kapoor, Optimal design of unitized panels with curvilinear stiffeners, in: Proceedings of the Aiaa Atio and Lighter-Than-Air Sys Tech. and Balloon Systems Conferences, 2005.
[20] A.Y. Tamijani, Buckling and stress analysis of curvilinearly stiffened plates using meshfree method, in: Proceedings of the AIAA/ASME/ASCE/AHS/ASC Structures, Structural Dynamics, and Materials Conference, 2009, pp. 2739–2751.
[21] A.Y. Tamijani, S.B. Mulani, R.K. Kapania, A framework combining meshfree analysis and adaptive kriging for optimization of stiffened panels, Struct. Multidiscip. Optim. 49 (2014) 577–594.
[22] D. Wang, M.M. Abdalla, W. Zhang, Buckling optimization design of curved stiffeners for grid-stiffened composite structures, Compos. Struct. 159 (2017) 656–666.
[23] A. Tounsi, M.S.A. Houari, S. Benyoucef, A refined trigonometric shear deformation theory for thermoelastic bending of functionally graded sandwich plates, Aerosp. Sci. Technol. 24 (2013) 209–220.
[24] A. Mahi, A. Tounsi, A new hyperbolic shear deformation theory for bending and free vibration analysis of isotropic, functionally graded, sandwich and laminated composite plates, Appl. Math. Model. 39 (2015) 2489–2508.
[25] K.S. Al-Basyouni, A. Tounsi, S.R. Mahmoud, Size dependent bending and vibration analysis of functionally graded micro beams based on modified couple stress theory and neutral surface position, Compos. Struct. 125 (2015) 621–630.
[26] S. Cheng, P. Qiao, F. Chen, W. Fan, Z. Zhu, Free vibration analysis of fiber-reinforced polymer honeycomb sandwich beams with a refined sandwich beam theory, J. Sandw. Struct. Mater. 18 (2016) 242–260.
[27] D. Bushnell, PANDA2—Program for minimum weight design of stiffened, composite, locally buckled panels, Comput. Struct. 25 (1986) 469–605.
[28] D. Bushnell, W.D. Bushnell, Minimum-weight design of a stiffened panel via PANDA2 and evaluation of the optimized panel via STAGS, Comput. Struct. 50 (1994) 569–602.
[29] F.W. Williams, M.S. Anderson, R. Butler, D. Kennedy, VICONOPT - program for exact vibration and buckling analysis or design of prismatic plate assemblies, AIAA J. 29 (1991) 1927–1928.
[30] G. Farin, Curves and surfaces for computer aided geometric design: a practical guide, 2014.
[31] J. Li, R.K. Kapania, W.B. Spillman, Placement optimization of distributed-sensing fiber-optic sensors using genetic algorithms, Grb Coord. Netw. 46 (2008) 824–836.
[32] P. Hao, B. Wang, K. Tian, G. Li, K. Du, F. Niu, Efficient optimization of cylindrical stiffened shells with reinforced cutouts by curvilinear stiffeners, AIAA J. 54 (2016) 1350–1363.
[33] S. Mulani, J. Li, P. Joshi, R. Kapania, Optimization of stiffened electron beam freeform fabrication (EBF3) panels using Response Surface Approaches, in: Proceedings of the 48th AIAA/ASME/ASCE/AHS/ASC Structures, Structural Dynamics, and Materials Conference, 2007.
[34] S.B. Mulani, W.C. Slemp, R.K. Kapania, EBF3PanelOpt: an optimization framework for curvilinear blade-stiffened panels, Thin-Walled Struct. 63 (2013) 13–26.
[35] K. Lakshmi, A.R.M. Rao, Optimal design of laminate composite isogrid with dynamically reconfigurable quantum PSO, Struct. Multidiscip. Optim. 48 (2013) 1001–1021.
[36] P. Hao, B. Wang, G. Li, Surrogate-based optimum design for stiffened shells with adaptive sampling, AIAA J. 50 (2012) 2389–2407.
[37] A. Kattan, R. Abdullah, A dynamic self-adaptive harmony search algorithm for continuous optimization problems, Appl. Math. Comput. 219 (2013) 8542–8567.
[38] S.L. Kang, W.G. Zong, A new structural optimization method based on the harmony search algorithm, Comput. Struct. 82 (2004) 781–798.
[39] M. Mahdavi, M. Fesanghary, E. Damangir, An improved harmony search algorithm for solving optimization problems, Appl. Math. Comput. 188 (2007) 1567–1579.
[40] Z.W. Geem, J.H. Kim, G.V. Loganathan, Harmony search optimization: application to pipe network design, Int. J. Model. Simul. 22 (2015) 125–133.
[41] M.G.H. Omran, M. Mahdavi, Global-best harmony search, Appl. Math. Comput. 198 (2008) 643–656.
[42] M. El-Abd, An improved global-best harmony search algorithm, Appl. Math. Comput. 222 (2013) 94–106.
[43] N. Sinsuphan, U. Leeton, T. Kulworawanichpong, Optimal power flow solution using improved harmony search method, Appl. Soft Comput. 13 (2013) 2364–2374.
[44] D. Havens, S. Shiyekar, A. Norris, R.K. Bird, R.K. Kapania, R. Olliffe, Design, optimization, and evaluation of integrally stiffened Al-2139 panel with curved stiffeners, 2011.
[45] I. Kaymaz, C.A. Mcmahon, A response surface method based on weighted regression for structural reliability analysis, Probabilistic Eng. Mech. 20 (2005) 11–17.
[46] S.C. Kang, H.M. Koh, J.F. Choo, An efficient response surface method using moving least squares approximation for structural reliability analysis, Probabilistic Eng. Mech. 25 (2010) 365–371.
[47] C.G. Bucher, U. Bourgund, A fast and efficient response surface approach for structural reliability problems, Struct. Saf. 7 (1990) 57–66.